Annals of Biomedical Engineering, Vol. 43, No. 1, January 2015 (© 2014) pp. 238–257
DOI: 10.1007/s10439-014-1180-8

Hemodynamics in the Microcirculation and in Microfluidics

TOSHIHIRO OMORI,[1] YOHSUKE IMAI,[1] KENJI KIKUCHI,[1] TAKUJI ISHIKAWA,[1,2] and TAKAMI YAMAGUCHI[2]

[1]Department of Bioengineering and Robotics, Tohoku University, Aoba 6-6-01, Sendai, Miyagi, Japan; and [2]Department of Biomedical Engineering, Tohoku University, Aoba 6-6-01, Sendai, Miyagi, Japan

(*Received 30 May 2014; accepted 4 November 2014; published online 15 November 2014*)

Associate Editor Umberto Morbiducci oversaw the review of this article.

Abstract—Hemodynamics in microcirculation is important for hemorheology and several types of circulatory disease. Although hemodynamics research has a long history, the field continues to expand due to recent advancements in numerical and experimental techniques at the micro-and nano-scales. In this paper, we review recent computational and experimental studies of blood flow in microcirculation and microfluidics. We first focus on the computational studies of red blood cell (RBC) dynamics, from the single cellular level to mesoscopic multiple cellular flows, followed by a review of recent computational adhesion models for white blood cells, platelets, and malaria-infected RBCs, in which the cell adhesion to the vascular wall is essential for cellular function. Recent developments in optical microscopy have enabled the observation of flowing blood cells in microfluidics. Experimental particle image velocimetry and particle tracking velocimetry techniques are described in this article. Advancements in micro total analysis system technologies have facilitated flowing cell separation with microfluidic devices, which can be used for biomedical applications, such as a diagnostic tool for breast cancer or large intestinal tumors. In this paper, cell-separation techniques are reviewed for microfluidic devices, emphasizing recent advances and the potential of this fast-evolving research field in the near future.

Keywords—Hemodynamics, Cellular flow, Computational fluid dynamics, Microfluidic devices.

INTRODUCTION

Blood is a dense suspension of blood cells, primarily consisting of red blood cells (RBCs), white blood cells (WBCs), and platelets (PLTs). Due to the presence of flowing cells in blood plasma, blood flow shows specific rheological properties and mass-transport phenomena. In microcirculation, especially, individual cell behavior is relevant to physiology and several pathologies of the microcirculatory system.[50,128] Cellular level hemodynamics is, thus, an attractive topic in the research field of biomechanics and bioengineering, with numerous theoretical, experimental, and computational studies having been conducted over the past 50 years. In particular, computational simulations of cellular flow have evolved rapidly over the last decade, and significant findings related to the dynamics of RBCs in fluid flow, the thickness of the cell-free layer in a capillary, margination of PLTs and WBCs, and adhesion to blood vessel walls have been published by many groups. In this paper, we review recent computational and experimental studies of blood flow in microcirculation and microfluidics (cf. Fig. 1). In "Cellular-Scale Computational Hemodynamics" section, we focus on RBC dynamics at the single cellular level, and then expand to mesoscopic multiple cellular flow in microvessels. Following "Computational Modeling of Cellular Adhesion" section, we review recent computational cell-adhesion models of WBCs, PLTs, and malaria-infected RBCs. In "Experimental Measurement of Cellular Scale Hemodynamics" section , the latest experimental visualization techniques for blood flow in microfluidics are described. In "Application of Hemodynamics to Microfluidic Devices" section, we review recent biomedical applications with microfluidic devices. We summarize this review in "Summary" section.

CELLULAR-SCALE COMPUTATIONAL HEMODYNAMICS

In microvessels, below diameters of 200 μm, it cannot be assumed that blood is a homogeneous continuum liquid; thus, individual RBC motion becomes important.[84,124] To simulate RBC motion and deformation accurately, the fluid-structure interactions of

Address correspondence to Toshihiro Omori, Department of Bioengineering and Robotics, Tohoku University, Aoba 6-6-01, Sendai, Miyagi, Japan. Electronic mail: omori@pfsl.mech.tohoku.ac.jp

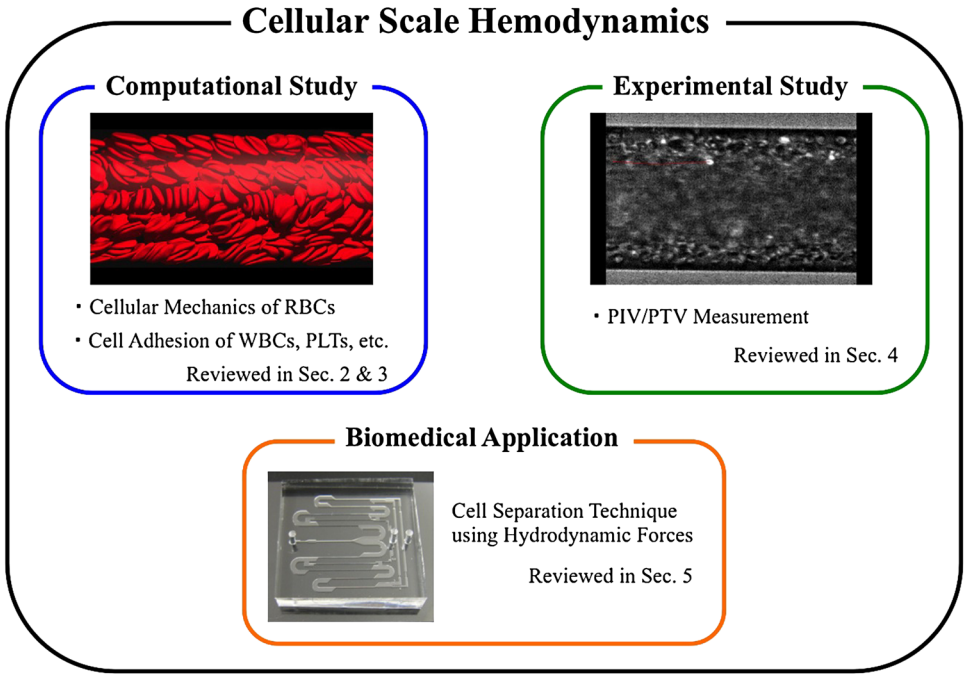

FIGURE 1. Outline of this review paper. In "Cellular-Scale Computational Hemodynamics" and "Computational Modeling of Cellular Adhesion" sections, we review recent computational studies. In "Experimental Measurement of Cellular Scale Hemodynamics" section, latest particle image velocimetry (PIV) and particle tracking velocimetry (PTV) measurement techniques are reviewed, and cell separation technique using hydrodynamic forces are reviewed in "Application of Hemodynamics to Microfluidic Devices" section.

the cell membrane and the fluid motion of the cytoplasm and blood plasma must be considered. In this section, we review recent cellular-scale computational hemodynamics from mechanical modeling of the RBC membrane to cellular flow in a large capillary.

Mechanical Modeling of the RBC Membrane

A human RBC has no nucleus, and consists simply of a cell membrane and the cytoplasm of the hemoglobin solution.[48,97] Thus, membrane mechanics is a crucial factor in RBC motion simulations of fluid flow. The membrane consists primarily of a lipid bilayer and a cytoskeletal elastic spectrin network. The lipid bilayer coupled to a network of spectrin protein gives rise to several important mechanical properties of the membrane, such as area incompressibility and high elasticity.

The plasma membrane is a lipid bilayer, and is responsible for the area incompressibility of the membrane.[44] Spectrin tetramers form 2D network structures on the membrane.[97] Due to the high elasticity of the spectrin network, the cell can pass through a narrow capillary, even when the diameter is smaller than the cell size. The thickness of the membrane is estimated to be 10 nm,[133] whereas the longest end-to-end length of the cell is 8 μm; thus, the membrane thickness is 1000 times smaller than the cell size. Continuum-based 2D membrane models are widely used for the thin shell structure of the RBC membrane.[12,37,125,133]

Several 2D constitutive laws have been proposed to model the mechanical behavior of a hyperelastic surface. The Mooney-Rivlin model[52] has been used for isotropic volume-incompressible rubber-like materials. For small deformation, the correspondence between the material properties and the law's parameters can be described as:

$$G_s = G_s^{MR},\ E_s = 3G_s,\ \nu_s = 1/2,\ K_s = 3G_s,$$

where G_s is surface shear elastic modulus, E_s is surface Young modulus, ν_s is surface Poisson ratio, and K_s is area dilation modulus. To express the large deformation and area-incompressible properties of a biological cell membrane, Skalak *et al.*[133] proposed the relationship between the material properties and the law parameters to be:

$$G_s = G_s^{SK},\ E_s = 2G_s\frac{2C+1}{C+1},\ \nu_s = \frac{C}{C+1},\ K_s = G_s(1+2C),$$

where $C \equiv K_s/G_s$ is the ratio between the two moduli. In the case of a RBC, the membrane is almost incompressible, and the moduli ratio C is on the order of 10^5.[125] All laws are reduced to the linear Hooke's law in the small deformation limit; however in larger deformations, each

law model has different material behaviors. The Mooney-Rivlin law shows strain-softening behavior under large deformation, whereas the Skalak law shows strain-hardening behavior under large deformation. Such qualitative differences in large deformation yield quantitative differences in material property estimations. For example, Dao *et al.*[27] and Takeishi *et al.*[140] numerically estimated the shear elastic modulus G_s of the RBC membrane, using the Mooney-Rivlin law and the Skalak law, respectively. In both studies, G_s was determined by comparing the results of an experimental optical tweezer stretching test.[139] The resulting value becomes $G_s = 13$ μN/m when the membrane is modeled with the Mooney-Rivlin law, whereas it is estimated as $G_s = 4$ μN/m for the Skalak law. Because the Skalak law can express the area-incompressible property, it is now widely used for the RBC membrane.

Many researchers have also used discrete spring network models to represent the membrane of capsules and biological cells.[87,101] One of the main advantages of such models is the simplicity of the mathematical description. To compare discrete spring network models and continuum constitutive laws, Omori *et al.*[107] investigated the mechanical properties of spring network membrane models. The authors concluded that spring network models do not express the area-incompressible properties of biological membranes, and that it is necessary to choose a membrane model that does, such as the Skalak law.

Although many studies have made efforts to clarify membrane mechanics, the stress-free reference shape of the RBC remains a big issue. In most computational studies, the reference shape is assumed to be a biconcave disk,[47,108,129,138] and several important RBC dynamics, such as tank-treading, tumbling, and swinging motions in simple shear flow, can be simulated using this assumption. Peng *et al.*[113] also numerically investigated RBC dynamics in shear flow using a multi-scale membrane model. The authors assumed a spheroidal stress-free shape in the cytoskeleton, instead of a biconcave shape, and reported that the cell maintained its biconcave shape during the tank-treading motion at a low shear rate. This type of motion corresponds to previous experimental observations,[32] but has not been reported in past numerical studies. Because a spherical stress-free shape cannot express swinging motions, it is possible that the stress-free shape is non-spherical; however, further investigations are needed to verify this presumption.

Dynamics of an RBC in a Simple Shear Flow

RBC dynamics in shear flow have been investigated by many researchers analytically,[104,134] experimentally,[1,32,43] and numerically.[108,109,129,138] In most computational studies, shear rate is normalized by capillary number, which expresses the ratio between the viscous stress of the fluid and the elasticity of the membrane. The capillary number is defined as $Ca = \mu a\dot{\gamma}/G_s$, where μ is viscosity of the surrounding liquid, a is the characteristic length of the cell, and $\dot{\gamma}$ is the shear rate. As described in the previous "Mechanical Modeling of the RBC Membrane" section, three kinds of motion have been reported in past numerical studies. In a very low Ca regime, the RBC shows a rigid tumbling-like motion, as shown in Fig. 2a. When the RBC is subjected to high Ca flow, the membrane is deformed to the flow direction and the membrane rotates around its shape, which is called tank-treading motion. If one assumes a non-spherical reference shape for the membrane, the RBC also oscillates with a half-time period of tank-treading motion in this regime (cf. Fig. 2b). This motion is called swinging motion, and has been reported experimentally.[1] If one uses a spherical stress-free reference shape, the RBC shows a steady tank-treading motion with no oscillation.[147]

In most past computational studies, the revolution axis of the biconcave disk was initially located in the shear plane, as shown in Figs. 2a and 2b. However, RBCs could be aligned in random directions in practical situations. Omori *et al.*[108] numerically investigated off-plane motions of the RBC using a coupled finite element/boundary element method (BEM). In their study, the revolution axis was initially located out of the shear plane, and the membrane was modeled using the Skalak law. As shown in Figs. 2c and 2d, the RBC dynamics changed qualitatively with capillary number. Under low Ca conditions, the revolution axis gradually drifted to the shear plane and finally converged to an in-plane swinging motion after a long time duration. In high Ca, however, the revolution axis drifted to the vorticity axis of the shear flow. Such reorientation phenomena have also been reported in other numerical studies[24,33] and in an experimental study.[32] However, the final converged orientation tends to differ between the Stokes flow regime and a finite Reynolds number flow regime with a non-identical viscosity ratio. For example, Cordasco and Bagchi[24] investigated off-plane motion of an oblate capsule and an RBC using a front-tracking with immersed boundary method. The membrane was modeled using the Skalak law, and the particle Reynolds number ($Re_p = \rho a^2\dot{\gamma}/\mu$) was set to 10^{-2}, while Stokes flow was used in Omori *et al.*[108]. Although the converged orientation is the same in the two studies when the viscosity ratio is identical, it becomes different in a high viscosity ratio regime (e.g., the revolution axis drifts to the shear plane in low Ca in Omori *et al.*, while it drifts to the vorticity axis in Cordasco and Bagchi). To fully

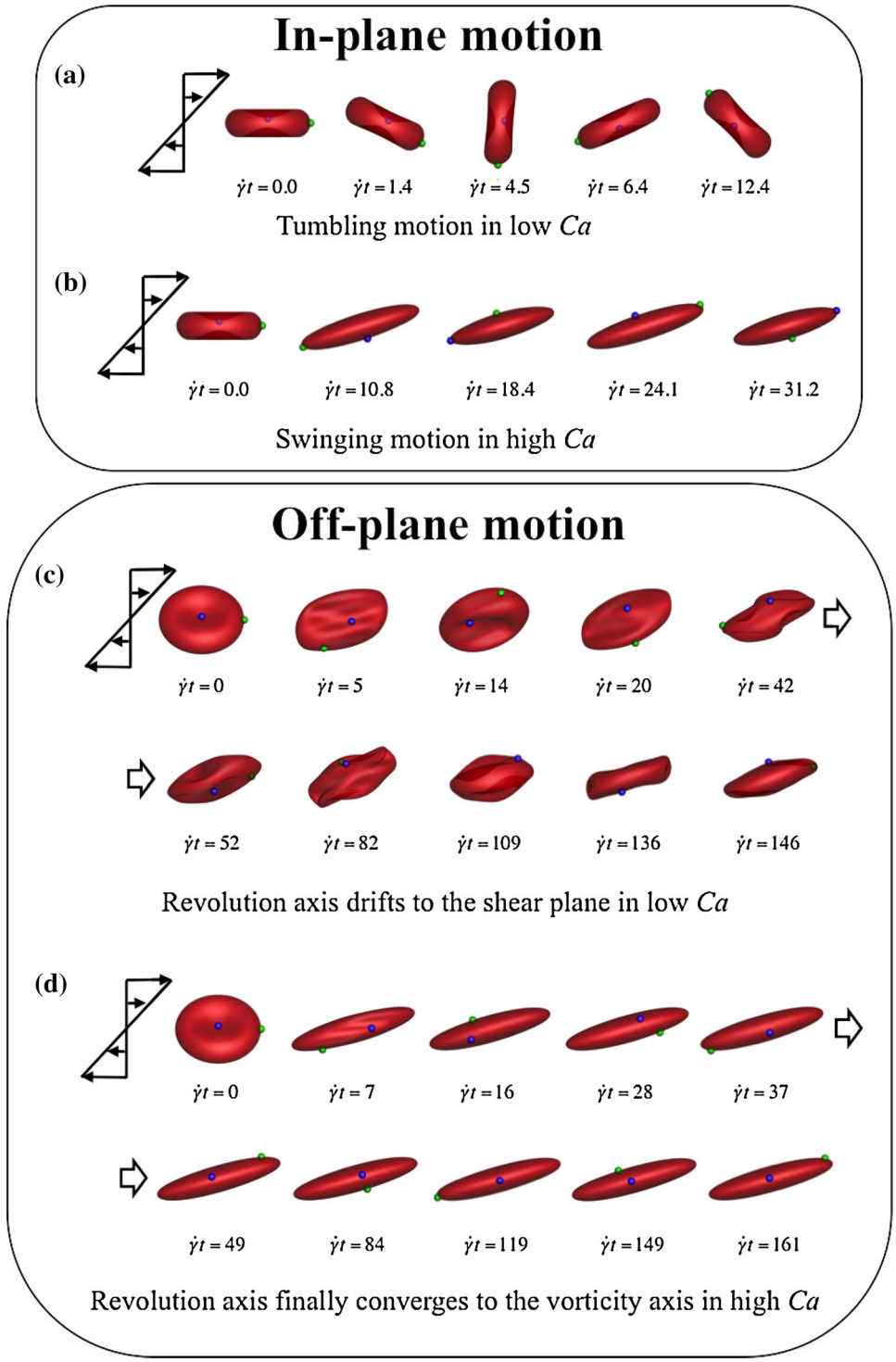

FIGURE 2. Time evolution of an RBC in shear flow. When the revolution axis of the biconcave disk, which is indicated as a blue dot, is initially located in the shear plane, the RBC shows tumbling or swinging motion depending on the capillary number (a: $Ca = 0.02$ and b: $Ca = 1.0$). While the revolution axis is initially located out of the shear plane, the RBC reorients to certain directions depending on the capillary number after long time duration, as shown in Fig. 2c ($Ca = 0.2$) and 2d ($Ca = 1.5$).[108] Green dot indicates a marker point on the membrane.

understand RBC dynamics in shear flow, RBC orientation should be considered, and the inertia and viscosity ratio effects need further investigation.

Tension of an RBC Under Fluid Flow

In numerical simulations of a capsule and RBC in shear flow, the membrane tension is often used as a

criterion for determining whether computation is stable. For example, Barthès-Biesel and co-workers numerically investigated membrane tension of a spherical capsule in a simple shear flow.[80,150] They found that when the capillary number became less than the threshold value Ca_L, negative tension appeared and the computation became unstable. When the capillary number was larger than Ca_H, negative tension again appeared at the tip of the deformed capsule, and the computation also became unstable. Thus, the stable computational parameter range is limited to $Ca_L < Ca < Ca_H$. If one uses the Skalak law for the capsule membrane, the criteria Ca_L and Ca_H become 0.4 and 2.4, respectively.[150] If one uses the neo-Hookean law, the criteria Ca_L and Ca_H become 0.45 and 0.63, respectively.[150]

Recently, Wan *et al.*[151] experimentally measured shear-induced adenosine triphosphate release from RBCs using a microfluidic device. A force-induced molecular release phenomenon was reported in *E. coli* cells,[163] and the mechanosensitive ion channel structure of bacteria was investigated. Although the ion channel structures of an RBC membrane are more complex than those of bacteria, membrane tension likely plays a role in the regulation of ion channels. Omori *et al.*[109] investigated RBC membrane tension under simple shear flow. Fluid flow was solved by a BEM, and the membrane was modeled using the Skalak law. The authors showed that the maximum principal tension during the tank-treading period increased linearly with respect to capillary number. This indicates that the maximum principal membrane tension can be estimated from the applied shear rate. For example, when the RBC is subjected to shear flow with a shear rate $\dot{\gamma} = 200\ s^{-1}$, the capillary number is equivalent to $Ca = 0.86$ (we use $G_s = 4\ \mu$N/m,[140] $\mu = 6$ mPa s,[48] $a = 2.85\ \mu$m[36]). In this case, the maximum principal tension can be estimated as 9 μN/m.[109] The details of mechanotransduction in the RBC membrane remain unknown. To fully understand them, it is essential to have pertinent information related to membrane tension, such as the threshold value needed to open a mechanosensitive ion channel.

Computational Study for Microfluidic Application: Membrane Stiffness Measurements

Single cellular RBC mechanics in a microfluidic device can be used to estimate membrane stiffness.[64] In this section, we will explain how to apply channel flow to measure membrane stiffness.

We consider a RBC flowing through a narrow circular capillary. The vessel radius R is equivalent to the cell size, and the length should be enough long to see developed flow in the channel. In microfluidics, typical mean velocity can be estimated as $U = 10^{-3}$ m/s, and the Reynolds number of the capillary flow is estimated as $Re = 2\rho UR/\mu \approx 10^{-2}$, where R is the vessel radius. Thus, the flow field is often viscous-dominant, and the inertia effect can be negligible. In this case, the capillary number can be rewritten as $Ca = \mu U/G_s$, the RBC motion becomes steady state, and deformation also becomes quasi-static after flow development. RBC deformation is determined by capillary number in the steady state, and we can estimate the shear elastic modulus from the relationship between deformation and capillary number. For example, Hu *et al.*[64] numerically estimated the membrane elastic modulus of a capsule using a narrow capillary flow. In the numerical simulation, the capsule membrane was modeled by the neo-Hookean law, and a BEM was used for the fluid mechanics. The results were validated by comparison with the experimental results of Lefebvre *et al.*[83] Lefebvre *et al.*[83] estimated the shear elasticity modulus using cylindrical pore measurements and found that $G_s = 0.07 \pm 0.01$ N/m, whereas the simulation result indicated 0.08 N/m.[64]

Hemodynamics in Microvessels

Next, we review recent computational cellular flows in capillaries. This field has evolved rapidly over the last decade, and several computational methods have been developed. A BEM is now widely used for cellular flow.[47,108,113,129] This method can explicitly treat viscous stress jump across the membrane, and is one of the most accurate computational schemes for tracking the interface. However, BEM is limited to a Stokes flow regime, and it is difficult to discuss an inertia effect. A lattice-Boltzmann method (LBM) is also widely used for cellular flow.[122,138,140] This method is fully explicit and no iterative solver is needed in the solving procedure. LBM can explicitly treat the inertia effect, unlike BEM, but the numerical accuracy using LBM becomes less than that with BEM, because LBM is often coupled with an immersed boundary method for tracking the interface, and physical quantities at the membrane, such as velocity and body force, are calculated using an interpolation function. Some researchers also use dissipative particle dynamics (DPD) to simulate RBC dynamics.[39,84] DPD particles represent virtual clusters of molecules, and unlike molecular dynamics, additional dissipative and random forces are considered. By including thermal energy in the random force, thermal fluctuations can be explicitly expressed. However, it often becomes less accurate in momentum conservation, comparing BEM and LBM, because DPD forces are just given as the sum of pair-wise interactions with neighboring particles. A moving particle semi-implicit method (MPS)

has also been used for simulating cellular flow.[4,147] In the MPS method, the Navier−Stokes equation is split into an advection-diffusion equation and a Poisson equation for pressure. Forces generated by cell deformation are substituted into the external force term. Thus, implementation of the fluid-structure interaction becomes simple, but this method is less accurate for computing the stress jump across the membrane.

Using the various numerical schemes above, the thickness of the cell-free layer and wall shear stress in microvessels has been investigated.[3,11,29,47,58,84,123] When the vessel diameter D is equivalent to the cell size ($D \simeq 8$ μm), the thickness of the cell-free layer becomes a function of U/D, where U is the mean velocity. Freund and Orescanin[47] numerically investigated the thickness of the cell-free layer using a BEM. The vessel size was set as $D = 11.3$ μm, and 12 RBCs flowed in the lumen. The authors reported that the thickness of the cell-free layer increased with U/D, but became approximately constant when $U/D \geq 100\text{s}^{-1}$. They also conducted a scaling analysis of the cell-free layer thickness by considering the force balance of the lubrication lift force and cell expansion pressure. The resultant cell-free layer thickness δ was proportional to $(U/D)^{1/3}$. This estimation is available when $0.6 \leq \delta$ [μm] ≤ 1.2.[47]

The cell-free layer is also a major factor that contributes to the Fahraeus-Lindqvist effect. To investigate the apparent viscosity of blood flow in a vessel diameter of 10–150 μm, various numerical schemes have been proposed and developed.[3,11,29,84] With cellular flow in a diameter of $D = 100$ μm with hematocrit 40%, we need to compute at least $O(10^3)$ of the RBCs, and a high-performance computing method is required. Although the modeling differs among the numerical studies (i.e., Alizadehrad *et al.*[3] used MPS for fluid motion and a spring network model for the membrane; Doddi and Bagchi[29] used a front-tracking and neo-Hookean membrane), and the apparent viscosity, as well as the cell-free layer thickness, often corresponded quantitatively with experimental studies.[76,127] This suggests that the apparent viscosity and the cell-free layer thickness may be primarily determined by macroscopic parameter, such as vessel diameter, flow rate, and hematocrit, rather than by precise microscopic cellular mechanics, such as the membrane mechanics and fluid motion around the cell.

In a large capillary, however, RBC dynamics vary with respect to local radial positions.[4,84] Alizadehrad *et al.*[4] quantified the radial variation in RBC deformation in a capillary of $D = 50$ μm with hematocrit of 20–45%. Due to the high local shear rate at the edge of the cell-free layer, the RBCs located near the wall were strongly deformed and oriented parallel to the flow direction, whereas the cells were weakly deformed around the center region. In larger capillaries (100–150 μm in diameter), local shear rate changed abruptly at the edge of the cell-free layer.[84] In the central core region, the local shear rate increased gradually as the radial position increased; however, it jumped at the cell-free layer edge.[84] To express 100 μm scale cellular flow using continuum mechanics, Lei *et al.*[84] proposed a Newtonian model with a velocity-slip boundary condition at the edge of the cell-free layer.

Rigorous cellular mechanics are also needed to discuss cell aggregation phenomena, because cell-cell interactions will be influenced by intercellular fluid motions. In most previous numerical studies regarding rouleaux formations;[42,84,164] however, simple potential functions were used to compute cell-cell interactions. To accurately predict rouleaux formation, we must solve hydrodynamic interactions between cells more precisely.

COMPUTATIONAL MODELING OF CELLULAR ADHESION

The adhesion of cells to the vascular wall is an essential process in various physiological functions. In the immune system, circulating leukocytes adhere to endothelial cells and then migrate into the tissue toward the infection site. PLTs adhere to the injured site of the wall and form a thrombus to stop the bleeding as a hemostasis response. Cellular adhesion also relates to a serious infectious disease—*Plasmodium falciparum* malaria. Although cellular adhesion is primarily mediated by ligand-receptor interactions of adhesion molecules, this problem also involves fluid and solid mechanics of cellular flow. In this section, we will review previous efforts on computational modeling of cellular adhesion to understand leukocyte and PLT functions and malaria infection.

Leukocytes

Leukocytes are spherical cells with microvilli on their surfaces. The volume of neutrophils is approximately 300 μm^3,[145] corresponding to a diameter of 8.3 μm. Due to the many folds and microvilli, the leukocyte membrane has excess surface area. Leukocytes are much less deformable than RBCs; their surface tension ranges from 0.024-0.035 mN m^{-1},[38,103] and their apparent bending rigidity is 1 to 2×10^{-18} J.[166] More importantly, the presence of nuclei and structural components results in highly viscous, non-Newtonian cell behavior. Micropipet aspiration experiments with a liquid drop model have predicted that the apparent

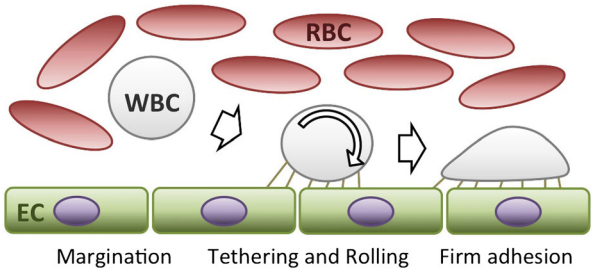

FIGURE 3. A multi-step process of leukocyte adhesion, consisting of margination, tethering, rolling and firm adhesion.

viscosity is approximately 60 Pa s for small deformations,[60] while it increases to 100-200 Pa s for large deformations.[38,60] Tran-Son-Tay *et al.*[146] modeled a leukocyte as a compound drop, in which the liquid drop of the cytoplasm had a small drop inclusion of nucleus; these drops had different viscosities and surface tensions. Their numerical simulation suggested that very high viscosity is not necessary for a cytoplasm to reproduce micropipet aspiration experiments if the surface tension and viscosity of the nucleus are assumed to be ten times higher than the cytoplasm.

A number of studies have been conducted on the adhesion process of leukocytes.[8] Leukocyte adhesion is a multi-step process consisting of margination, tethering, rolling, and firm adhesion as shown in Fig. 3. Although leukocytes are much less deformable than RBCs, they still experience some deformation. In the absence of hydrodynamic (collision) forces from RBCs, leukocytes move to the center of microvessels by lift forces due to the wall and shear gradient. Schmid-Schönbein *et al.*[132] observed that RBCs passed a leukocyte in microvessels larger than 10 μm, and proposed that the leukocytes are marginated by hydrodynamic forces from RBCs during the passing motion. Freund[46] developed the first numerical model of leukocyte margination using a BEM, where a leukocyte and RBCs were modeled as 2D capsules. Although early experimental studies[53,105] have suggested that RBC aggregation is necessary for leukocyte margination in large microvessels, numerical simulations showed that aggregation of RBCs is not a necessary condition for margination. The most efficient hematocrit range was investigated using DPD in.[41] Optimal margination could be obtained in the hematocrit range of $0.2 < Hct < 0.4$. In 2D simulations, a cell is modeled as an infinitely long cylinder. Correspondingly, a microvessel can be modeled by infinite parallel plates in 2D. However, 3D simulations are necessary for quantitative understanding of cellular flow. Due to the heavy computational load required when solving the hydrodynamic interactions between a leukocyte and many RBCs, 3D simulations have not been reported until recently.[41,140] To accelerate 3D simulation, graphics processing unit (GPU) computing was used effectively by Takeishi *et al.*[140] They showed that margination occurs, even for arteriole shear rates; however, the separation distance between the leukocyte and the wall surfaces may not be small enough for tethering with arteriole shear rates.

Tethering and rolling of leukocytes are primary mediated by selectin-ligand bindings, while firm adhesion is mediated by integrin-ligand bindings. A mathematical model of the association and dissociation of such ligand-receptor bindings was proposed by Bell.[13] In the Bell model, for example, the dissociation rate is described as a function of the unstressed dissociation rate, the binding force, the reactive compliance, and the thermal energy, where reactive compliance is a parameter that sets the sensitivity of a bond to dissociation to a force.[59] The unstressed dissociation rate and reactive compliance for the Bell model are obtained from experiments,[6,135] summarized in Table 1. Hammer and colleagues[59] developed a Monte Carlo simulation for adhesive dynamics,[59] in which the probability of association/dissociation for a single bond over each time interval is calculated using the Bell or Dembo models.[28] The Monte Carlo simulation has been coupled with a number of leukocyte models. Chang *et al.*[19] modeled a leukocyte as a rigid sphere; the Monte Carlo simulation was coupled with the motion of the rigid sphere near the wall. They presented a phase diagram of the behavior of leukocytes for a dissociation rate ranging from 10^{-3} to 10^{3} s^{-1} and a reactive compliance of 0.01 to 5 Å. They also showed how the phase diagram changes with different association rates and shear rates. Although these early studies ignored the deformation of leukocytes, a 2D capsule model of leukocytes with a Dembo model predicted that leukocyte deformability significantly altered the rolling velocity of leukocytes.[30] The nucleus also affects the rolling velocity. Comparison of a compound drop model with a simple drop model showed that the presence of a nucleus prolongs the bond lifetime and decreases the rolling velocity of leukocytes.[102] 3D simulations have been recently performed with the IBM,[69,110] or the volume-of-fluid (VOF) method.[73] For example, Khismatullin and Truskey[73] used a compound viscoelastic drop model of leukocytes to quantify the effect of cytoplasm and nuclear viscosities on leukocyte rolling.

A classical question is why leukocyte rolling and adhesion are often found in venules, but rarely in arterioles. Rolling and adhesion of a single leukocyte on a planar wall has been successfully simulated, but such simulations do not fully answer this question for the following reason. Many differences are present between venules and arterioles, including the geometry

TABLE 1. Unstressed dissociation rate and reactive compliance for the Bell model.

	Unstressed dissociation rate (s^{-1})	Reactive compliance (Å)
L-selectin	2.8–7.0	0.24 –1.11
P-selectin	0.93–2.4	0.39–0.4
E-selectin	0.7–2.6	0.31

of the vessels, such as bifurcations and confluences, the shape of endothelial cells, and the distribution of adhesion molecules. The presence of RBCs, in addition, affects the dynamics of leukocytes, as indicated by studies on leukocyte margination.[41,140] To fully understand adhesive phenomena of leukocytes, more experimental data on adhesive dynamics at the cellular scale are needed.

Platelets

Resting PLTs have discoid shapes with diameters of 2 μm, and become irregularly shaped when activated. PLTs are anuclear, but are composed of cytoplasmic components of megakaryocytes. Compared to RBCs and leukocytes, few studies have attempted to quantify the rheological properties of PLTs. Haga *et al.*[57] performed a micropipet aspiration experiment, and determined the apparent Young's modulus to be 1.7×10^2 *Pa*, and the apparent viscosity to be 1000 Pa s.

Margination has also been observed in PLTs.[144] The near-wall concentration of PLTs is higher in arterioles than venules.[158] In addition, the factors influencing margination are different from those that influence leukocytes.[155] Computational studies on PLT margination began with 2D models.[5,26] Crowl and Fogelson[26] modeled RBCs and PLTs as biconcave capsules and less deformable spherical capsules, respectively. Their simulation by LBM-IBM analysis demonstrated that a higher shear rate gives a faster rate of PLT transport to the cell-free layer, and a larger near-wall excess of PLTs. They also quantified PLT diffusion and proposed a drift diffusion model for PLT margination. Zhao and Shaqfeh[165], developed a 3D model, in which RBCs and PLTs were modeled as capsules and rigid discoids, respectively. The motions of these particles were precisely described by the BEM, and the relationship between PLT diffusion and the deformation of RBCs was evaluated.[165],

Tethering and rolling of PLTs is mainly governed by the interaction of the glycoprotein Ib/IX/V receptor complex (GPIb/IX/V) with the glycoprotein von Willebrand factor (vWF) bound to subendothelium (collagen). PLTs are activated during rolling, and GPIIb/IIIa (integrin $\alpha_{IIb}\beta_3$) then binds to vWF for firm adhesion. In PLT aggregation, GPIb/IX/V also binds to vWF, and GPIIb/IIIa binds to vWF or fibrinogen.[130] Some parameters in the Bell model were estimated by experiments; for example, the dissociation rate is 5.47 s^{-1}, and the reaction compliance is 0.71 nm for GPIb/IX-vWF bindings.[9] Mody and King[96] proposed a 3D model of two-platelet aggregation. They used BEM for the motion and hydrodynamic interaction of PLTs and a Monte Carlo simulation for GPIb/IX/V-vWF interactions, where PLTs were modeled as rigid discoids.

For large-scale PLT adhesion and aggregation, a continuum model was proposed by Fogelson and colleagues.[45] They coupled the Navier−Stokes equation for blood flow with the advection-diffusion equation for the concentration of PLTs. Particle models were also proposed for simulating a primary thrombus, including a distinct element method,[95] a Stokesian dynamics method,[99] and a MPS method.[70] These studies suggested that both the GPIb/IX/V-vWF and GPIIb/IIIa-fibrinogen bindings are necessary for the development of thrombus height. Recent models also consider the activation of PLTs,[118] and the characteristics of PLT glycoprotein receptors[72] for PLT adhesion and aggregation. For example, Kamada *et al.*[72] extended their early model[70] to include the characteristics of PLT glycoprotein receptors, and investigated thrombogenesis under pathological conditions, mimicking Bernard–Soulier syndrome and Glanzmann thrombasthenia, and also the effect of shear-induced PLT aggregation on thrombus growth.

While the presence of RBCs was ignored in the models mentioned above, Mori *et al.*[100] showed that the hydrodynamic forces from RBCs increase the number of PLTs involved in a thrombus slightly with horizontal spread of the thrombus, while inhibiting the vertical growth. The 3D simulation by Pivkin *et al.*[119] showed similar results. However, these studies[100,119] still have the problem that RBCs were modeled as rigid spheres. When the deformability of RBCs is considered, RBCs do not affect the height or coverage of a thrombus, whereas the extent of RBC deformation increases slightly if thrombi are diffusely formed in microvessels.[71] Recent studies have also tackled more realistic problems, including a direct comparison with experimental results *in vivo*,[154] and the complex coagulation cascade.[153,161]

Malaria Infected RBCs

Malaria is still one of the most serious infectious diseases. The malaria parasite, *Plasmodium falciparum* (*Pf*) grows within an RBC during the ring, trophozoite, and schizont stages.[94] Proteins exported by the parasite modify the membrane structure. *Pf*-infected RBCs

(*Pf*-IRBCs) become less deformed,[51] changing their shape to one that is more spherical than biconcave.[35] Surface knobs appear on the *Pf*-IRBC in the early trophozoite stage; the number of knobs increases as the parasite grows, reaching 7 μm^{-2} at the schizont stage.[85] The ligand mediating adhesion is *Plasmodium falciparum* erythrocyte membrane protein 1 (PfEMP1), expressed on the knob surface.[90] PfEMP1 interacts with a variety of endothelial receptors, such as ICAM-1 and CD36. *Pf*-IRBCs also adhere to healthy RBCs, a phenomenon called rosetting.

Suresh *et al.*[139] performed a stretching of *Pf*-IRBCs with optical tweezers, where axial and transverse diameters were measured as a function of applied forces. They compared the experimental results with those obtained from a finite element method (FEM) simulation to characterize the surface shear elastic modulus G_s; the estimated values were 5.3, 16.0, 21.3, and 53.3 $\mu N\ m^{-1}$ for the healthy, ring, trophozoite, and schizont stages, respectively. Note that these values should depend on the constitutive equation used in the model. When the Skalak constitutive law is used with a high-area dilation modulus $K_s = G_s(2C + 1)$ with $C = 100$, we estimated the value to be $G_s = 4.0\ \mu N\ m^{-1}$ for healthy RBCs.[140] In addition, the effect of rigid parasites on the deformation of *Pf*-IRBCs has also been reported.[62]

The first numerical model on the behavior of *Pf*-IRBCs in microcirculation was proposed by Kondo *et al.*[77] In this model, a spectrin network model was used for membrane mechanics, and the MPS method was used to study the fluid mechanics of plasma and cytoplasm. Because no data were available for the parameters of the Bell model, a simple spring model was used to describe the ligand-receptor interactions in cytoadhesion and rosette formation. This model was extended to three dimensions and used to study how the apparent viscosity of the blood flow changes with parasite growth.[66] Imai *et al.*[67] also investigated margination of *Pf*-IRBCs, and showed that a *Pf*-IRBC in the trophozoite stage, followed by healthy RBCs forming a train and their subsequent motion, effectively induced margination of the *Pf*-IRBC, similar to the leukocyte margination reported by Schmid-Schönbein *et al.*[132]. Fedosov *et al.*[39] incorporated the Monte Carlo method for ligand-receptor interactions in the DPD method for cellular flow.[39] They simulated the rolling motion of a *Pf*-IRBC on a wall coated with purified ICAM-1, in which the dissociation rate was set to 100 s^{-1}. At low shear rates, the simulated rolling velocity followed that obtained from experiments;[7] however, there were some discrepancies at high shear rates, prompting the proposal of a wall-shear, stress-dependent spring constant model for PfEMP1-ICAM-1 bindings,[40] More recently, Li *et al.*[86] quantified the dissociation rate and reactive compliance using atomic force microscopy, with values of 0.0013 s^{-1} and 0.75 nm for CD36 and 0.14 s^{-1} and 0.37 nm for TSP; the values for ICAM-1 have yet to be determined.

EXPERIMENTAL MEASUREMENT OF CELLULAR SCALE HEMODYNAMICS

The individual behavior of RBCs in blood flow has enabled these cells to be used in the diagnosis of blood diseases, such as a hemolysis and microvascular malaria infection. However, it can be difficult to observe blood flow. This is due to the absorption by the hem-protein of RBCs, with its high-density hematocrit level (Hct = 45% for healthy humans) for a capillary blood vessel over 100 μm in diameter. There have been many studies that focused on the development of new, convenient optical microscopic methods. In early research requiring blood-flow measurements, only optical microscopes were available to investigate microcirculation in animals. Thus, these first methods provided only a qualitative understanding of blood flow. Quantitative information, such as rheological effects and blood cell deformability, were difficult to obtain due to the lack of time and spatial resolution. For example, although the flow velocity is on the order of millimeters or micrometers per second, this corresponds to tremendously high speeds in the microscope's field of view. High-speed, high-resolution cameras with an enhanced sensitivity and mounted to an optical microscope enabled velocity measurements of such small-scale flows. Several techniques have been developed to measure the velocity fields at the micro-scale. These include digital imaging tools, such as PTV and PIV, as well as holographic techniques. With microscopic observation, these methods facilitated detailed investigation of the velocity fields of microfluidics and microcirculation for bioengineering and medical sciences. Although these velocity-measuring techniques have had many successes, there are several issues requiring further attention, such as the selectivity of tracer particles and the labeling method for blood or blood cells (Table 2). In the following section, we review established techniques for blood flow visualization for *in vivo* and *in vitro* situations, specifically, micro-PIV and PTV measurements of blood flow.

Micro-PIV Measurement for Blood Flow

Micro PIV (μPIV) is a common method for measuring blood flow at the micro-scale, *in vitro* as well as *in vivo*. μPIV has been successfully developed at this level by combining a conventional PIV system (a velocity analysis system that measures the local

TABLE 2. Selective stain for visualization of blood cell and flow.

Flow	*In Vivo*/*Vitro*	Observation (size, μm)	Method	Animal	Tracer particle (dye; ex/em)	d_p (μm)	Hct (%)	Author, year
Whole blood	*Vivo*	Arterioles (15−25)	Manual tracking	Rabbit	Labeled RBCs (FITC:490/525)	~ 8	25–35	Tangelder *et al.*[143]
	Vitro	Microchannel (100)	PTV	Human	PS particle (F8888:505/515)	1	10	Lima *et al.*[88]
	Vivo	Micro vessel (75-150)	PIV	Chicken embryo	RBCs (none)	~ 7	34	Poelma *et al.*[121]
Plasma	*Vitro*	FEP circular microtube (100)	PIV	Human	PS particle (-:427/468)	1	21	Sugii *et al.*[137]
	Vivo	Mesentery	PIV	Rat	PS particle (Fluo-max red:542/612)	0.5	36–54	Ha *et al.*[56]
	Vivo	Micro vessel (75-150)	PIV	Chicken embryo	PEG coated PS particle (Rhodamine B:550/570)	1.28	34	Poelma *et al.*[121]
RBC	*Vivo*	Mesentery	Manual Tracking	Rabbit	RBCs (none)	~ 7	30–50	Koutsiaris and Pogiatzi[78]Ha *et al.*[56]
	Vitro	Circular⁻ Microchannel (100)	PTV	Human	Labeled RBCs (DiC_{16}:549/565)	~ 7	21	Sugii *et al.*[137]
	Vitro	Circular⁻ Microchannel (50,100)	PTV	Human	Labeled RBC (CM-DiI:553/570)	~ 7	2–35	Lima *et al.*[88]
	Vivo	Micro vessel (75–150)	PIV	Chicken embryo	RBCs (none)	~ 7	34	Poelma *et al.*[121]
WBC	*Vivo*	Arterioles	Manual tracking	Rabbit	Labeled WBCs (FITC:490/525)	~ 14	25–35	Tangelder[143]
	Vivo	Micro vessel	PTV	Mouse	eGFP (485/530)	~ 14	39–49	Pickard and Ley[115]
Platelet	*Vivo*	Arterioles (15–25)	Manual tracking	Rabbit	Labeled platelet (Acridine red: 525/625)	~ 2	25–35	Tangelder *et al.*[143]

The particle image velocimetry (PIV) and particle tracking velocimetry (PTV) methods were applied to measure the blood flow, where were in micro scale vessel or channel *in vivo* and *in vitro*, *PS:Polystyrene.

velocity taken by the spatial cross-correlation differences between a pair of digital images) with epi-fluorescent microscopic observations using fluorescent tracer particles.[92,131] The microscale flow must be measured without the sensor inside the channel, i.e., a low-invasive flow measurement technique and equipment must be used, such as a thermo-anemometer or a pressure technique.

The selectivity of tracer particles has an important role in the measurement of microchannel flow because the size of a particle affects the traceability of the flow around the particle. In particular, the density of a tracer particle changes the viscosity of suspended fluids, as predicted by Einstein's viscosity equation, $\mu = \mu_0(1 + 2.5\phi)$,[34] where μ is the viscosity of the suspended fluids, μ_0 is the initial viscosity of the fluids, and ϕ is the particle volume concentration. In many cases for PIV measurements, the change in the viscosity is usually less than 1%, corresponding to 0.4% in particle volume concentration. This viscosity fluctuation is equivalent to approximately 0.5 K in fluid temperatures, based on the Andrade viscosity equation, $\mu = \mu_0 \exp(-cT)$. Here, c is the thermal coefficient ($c_{\text{water}} = 0.020$) and T is the temperature of the fluids. The particle volume concentration usually used is less than 0.4%. In fact, this concentration should be less than 0.1% and the particle size should be less than 1 μm using the μPIV method.[93,106] But although the μPIV method has the advantage of measuring velocity in micro flows, the spatial resolution is limited due to the diffraction limit and other optical issues. The spatial resolution, Δx, for μPIV depends on the optical parameters, as given below:[2]

$$\Delta x = \frac{1}{10M}\left[M^2 d_p^2 + 1.22M\frac{\lambda}{N_A}\right]^{1/2}, \qquad (1)$$

where M is the magnification of the objective lens, d_p is the mean diameter of the tracer particle, λ is the wavelength of the illuminating light, and N_A is the numerical aperture of the objective lens. Since peak intensities of the charge-coupled device (CCD) and complimentary metal-oxide-semiconductor image sensor (CMOS) are available with the green light, $\lambda = 560$ nm is now widely used. The axial resolution in micro PIV method, δ_z, is given by.[93]This depth size is direct related to the 2D velocity measurements in the flow field as light sheets in macro PIV methods:

$$\delta_z = \frac{n\lambda}{N_A^2} + \frac{ne}{MN_A}, \qquad (2)$$

where n is the refractive index of the immersion medium between the observed sample and the objective lens and e is the smallest resolvable distance of the image sensor. The blood flow was visualized within δz

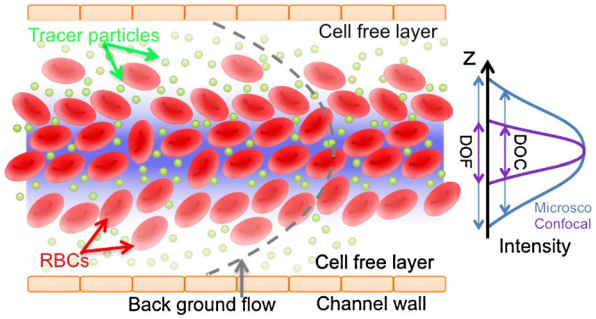

FIGURE 4. Schematic diagram for the visualized slice thickness for microscopic observation of depth of field (DOF) and effective thickness for PIV measurements of depth of correlation (DOC) based on the fluorescent particle size.

μm in thickness, which is related to the optical condition as depth of field (DOF), as shown in Fig. 4. The flow field can be observed according to Eq. (2), which can help in considering the experimental conditions; for example, the magnification of the objective lens and the height of the micro channel. The measured velocity using a couple of PIV images to calculate the cross-correlation algorithm, however, is needed to consider the effect of the out-of-focal plane, taking into account the depth of correlation (DOC):[156]

$$DOC = \frac{1}{2}\left[\frac{1-\sqrt{\varepsilon}}{\sqrt{\varepsilon}}\left(\frac{n^2}{N_A^2}-1\right)\left(d_p^2+\frac{1.49(M+1)^2\lambda^2}{M^2N_A^2}\right)\right]^{1/2}, \quad (3)$$

where ε is the minimum intensity of the tracer particles in the PIV images, which is usually applied at 10% of the intensity of an in-focus particle. If the DOC is calculated as the entire depth of the channel, then the in-plane velocity appears as the projected velocity, which is averaged in DOC. More detailed out-of-focus effects were discussed in terms of the theoretical pathway and optic parameters by Olsen and Adrian.[106] To improve the axial resolution of microscopic observations, a confocal scanner has been installed on a μPIV system to obtain a thin focal plane.[111,157] In a microtube flow, the ratio of the internal diameter of the circular channel and the diameter of the tracer particles should be less than 0.01 for precise accuracy of the Hagen-Poiseuille flow, with the particle volume ratio being 0.2%.[74] Using these values, the velocity errors are less than 7% near the circular channel wall for microtube diameters of 25, 50, and 100 μm.

The μPIV method has been used for *in vitro* blood-flow measurements with fluorescent microscopic observation. Sugii *et al.*[136] measured the velocity profile in microvessels of rat mesenteric arterioles using transparent microscopic imaging. The microscopic shadows of RBCs in the blood flow were used for velocity analysis in PIV methods, without any labeled cell or tracer particles. Thus, there are some advantages to ignoring the biological interactions and side effects of the animal conditions in *in vivo* experiments. The nano-tracer particles were more suitable for measuring flow velocities near the wall than RBCs as tracer particles, *in vitro*[117] as well *in vivo*,[121] because the cell-free layers near the wall have no traceable RBCs due to lateral migration. Poelma *et al.*[121] also mentioned that the velocities at the center of the micro vessel measured using tracer particles or RBCs tended to be almost the same in the case of high-magnication observations, depending on the numerical aperture of the objective lens. Some groups have succeeded in measuring the blood flow in *in vivo* experiments using μPIV methods with respect to the hearts of a zebra fish,[63] the embryonic venous vessels of a chicken,[61,82] and the vitelline network of a chicken.[120] In particular, *in vivo* whole-field blood velocity measurement techniques were reviewed by Vennemann *et al.*[149] For example, stealth tracer particles were used to measure the *in vivo* velocity fields of the ventricle of a chicken embryo by Vennemann *et al.*[148] to investigate the immune reactivity of animals.

Lima *et al.*[88] measured blood-cell suspension flow using a confocal μPIV method. They extended the 2D velocity profile of cell suspension flow in a square microchannel to 3D flow fields by measuring several heights of focal planes. Recently, Chen *et al.*[21] applied optical coherence tomography (OCT) to μPIV measurements to measure the *in vivo* blood flow of extra-embryonic vitelline. This OCT method was capable of measuring the velocity profile in the lateral direction, similar to ultrasonic sonar, with similar spatial resolution as that of conventional μPIV methods.

For more accurate velocity measurements for μPIV a pre-process and post-process were used. Pitts *et al.*[116] demonstrated the pre-processing method of image-overlapping blood flow compared with other base-clipping and thresholding methods. In their results, the image-overlapping method was most effective for calculating the flow profile of blood flow. Chayer *et al.*[20] demonstrated that the comparison of blood flow profiles measured by the μPIV method when the RBC was used as the tracer particle between *in vitro* experiments and *in silico* simulated one to assess the effects of DOC. In their results, both estimated flow rates, *in vitro* and *in silico*, were in good agreement, with less than 10% error, considering that DOC affected strongly the image processing to estimate the flow velocities.

Particle Tracking Velocimetry for Blood Flow

Measuring the blood flow at the microscale to investigate the behavior of blood cells was initially

performed by visualizing an illuminated transparent volume with optical microscopy using labeled RBCs as tracer particles. Tangelder *et al.*[143] visualized the *in vivo* blood flow in the arterioles of the rabbit mesentery using labeled blood cells, such as RBCs, WBCs, and PLTs, *via* fluorescein isothiocyanate (FITC) and acridine red dyes. They recorded weak fluorescent images of labeled blood cells using a high-sensitivity video camera and analog videotape. The velocity profile in the vessel was determined using the velocity of both of the RBCs and PLTs. These velocities were measured individually from the change in position over a time-step divided by the exposure time. Each velocity profile was parabolic, although the velocities for the RBCs were slower than the maximum speed of the PLTs. Koutsiaris *et al.*[78] investigated the axial RBC velocity pulse using a high-speed video microscopy method, and measured the velocity pulsation in terms of the change in time of the intensities at the center of the blood vessel based on the visualized blood flow images. Sugii *et al.*[137] performed *in vitro* experiments to track labeled RBCs dyed by $DiIc_{16}$ for a velocity profile analysis in a circular microchannel, 100 μm in diameter, using the PTV method. They also measured the velocity profile of plasma in blood flow for comparison with RBCs and concluded that both velocity profiles were in good agreement with the results obtained considering Poiseuille's flow. Kikuchi and Mochizuki[75] measured the RBC flow in the proboscis of a mosquito during blood suction using PTV methods; axis migration of the mosquito's proboscis was not observed during their experiments. Ha *et al.*[56] using a hybrid of PIV and PTV blood-flow profiles to examine the periodic change in the velocity in rat mesenteric vessels. WBCs have the role of protecting the body from infection and foreign material, a well-known immunoreaction. The adhesion of WBCs has recently focused on mechanotransduction and phagocytosis to cancer cells, as well as the autophagy mechanisms. Pickard and Ley[115] performed several studies to facilitate visualization of the flow around a WBC adhered to a blood vessel in an attempt to determine the shear stress on the surface. The flow around a WBC curved with the WBC surface, and the shape of the flow gradually became deformed. Fu *et al.*[49] succeeded in observing the flow around tumor cells adhered to the WBC in *in vitro* experiments.

APPLICATION OF HEMODYNAMICS TO MICROFLUIDIC DEVICES

Due to recent advances in micro total analysis system (μTAS) technologies, it is now possible to manipulate, stimulate, and diagnose cells using microfluidic devices.[23,159] A wide variety of techniques for cell separation has been proposed so far.[55,126] Fluorescence-activated cell sorting (FACS), for example, separates cells based on fluorescent labeling. A labeled cell is detected by laser light scattered by the cells, and collected using the electrostatic force acting on a drop containing the cell. Magnetic-activated cell sorting (MACS) separates cells based on antibody-conjugated magnetic beads. Specific proteins on a cell bind to the magnetic beads; then, the cell can be separated by an external magnetic field. Although these conventional labeling techniques have been successful, there are several disadvantages, such as long processing times, bulky apparatus, and complex preparation procedures. Recently, in an attempt to overcome these problems, label-free separation methods have been proposed by many researchers. Especially, microfluidic devices using mechanical forces for cell separation have attracted significant attention. The advantages of using mechanical forces are the simple preparation procedures and the small amount of space required for the apparatus. The mechanical forces induced on cells depend on the differences in the intrinsic physical properties of the cells, such as their size, shape, elasticity, plasticity, and viscosity. These mechanical force devices guide certain cells to designated outlets of the microfluidic devices using the difference in the mechanical forces exerted on each cell.

Microfluidic Devices for Blood-Cell Separation

When a cell flows in a microfluidic device, hydrodynamic forces always play an important role in the cell's behavior. Thus, hydrodynamic forces have been used for cell separation by many groups. Yang *et al.*[162] developed a microfluidic device for continuous blood plasma separation using the bifurcation law, known as the Zweifach-Fung effect. The bifurcation law states that a particle around the stagnant region of bifurcation tends to flow into the daughter channel at a higher flow rate. Petersson *et al.*[114] used acoustic forces in a standing wave field to separate lipid particles from RBCs in whole blood. The acoustic forces were generated in different directions for the two types of particles due to the differences in their compressibility and density. The developed device achieved approximately 70% separation efficiency for the lipid particles. Gorkin *et al.*[54] reviewed centrifugal microfluidic devices for biomedical applications. Plasma separation from whole blood using a centrifugal microfluidic device has been successfully performed by several groups. Chen *et al.*[22] separated WBCs and RBCs using pillar-type and weir-type filtration microchips. These devices were based on cross-flow filtration using the size differences between cell types. Moon *et al.*[98] developed a micro-

fluidic device for the separation of cancer cells from blood cells by combining multi-orifice flow fractionation and dielectrophoretic cell separation techniques. They succeeded in enriching cancer cells up to about 160-fold. RBCs and WBCs were efficiently removed with high separation efficiencies.

Recently, several groups have developed state-of-the-art microfluidic devices based on inertia-induced migration forces.[14,18,112,141] When a particle flows parallel to a wall with a non-negligible inertia effect, the particle experiences an inertia-induced lift force perpendicular to the wall. Asmolov *et al.*[10] calculated the inertia-induced lift force F_L of a rigid sphere flowing in a straight circular tube by asymptotic analysis. They derived F_L as $F_L \propto \rho\dot{\gamma}a^4$, where ρ is the density, $\dot{\gamma}$ is the shear rate, and a is the radius of the sphere. Note that the inertia-induced lift force is proportional to the radius to the *fourth* power. Thus, slight differences in the cell size can be amplified strongly, and sorting due to size difference becomes possible. The counterpart of the lift force is the inertia-induced drift force that drives particles away from the channel center towards the walls. Both the lift force (away from the wall) and the drift force (towards the wall) are generated by the inertia effect. The acting directions of the two forces are opposite, because the particle interacts with different flow conditions, i.e. no slip boundary condition on the wall or constant shear gradient in Poiseuille flow. The main advantage of using the inertial force is that the flow velocity can be significantly larger than other methods, resulting in higher throughput of the device.

Several groups have succeeded in using inertia-induced lift forces for medical applications. Hur *et al.*[65] designed a microfluidic device consisting of 256 high-aspect parallel channels to prevent the overlap of cell images using inertial migration forces. They conducted automated RBC and leukocyte counts on diluted blood, and achieved high counting sensitivity and specificity. Carlo *et al.*[17] developed similar microfluidic devices for separating rigid particles, deformable emulsions, and PLTs from whole blood. They showed that cascading separations in series is effective for improving separation purity. Wu *et al.*[160] separated bacteria from human blood cells by inertial forces. They used a combination of an asymmetrical sheath flow to generate the inertial force, and achieved a 300-fold enrichment of bacteria over a wide range of flow rates. Mach and Carlo[89] developed a parallel microfluidic device that separates pathogenic bacteria from diluted blood; each channel consisted of a short focusing, gradual expansion, and collection regions. They again used the inertial lift forces for cell separation, and removed about 80% of pathogenic bacteria from the blood.

Microfluidic Devices for Separation of Cancer Cells from Blood

Inertia-induced lift force has also been used to separate cancer cells from blood. The reason why some researchers are interested in this phenomenon is because a circulating tumor cell (CTC) test has been recognized as a new diagnostic tool to evaluate the prognosis or cure effect of breast cancer or large intestinal tumors.[16,25] In a CTC test, the patient's condition is diagnosed by the number of cancer cells in a certain volume of a peripheral blood sample; the separation of the cancer cells is the key technology. Kuntaegowdanahalli *et al.*[79] reported a microfluidic device for multi-particle sorting using inertial migration forces in spiral microchannels. In the case of a curved channel, centrifugal force (Dean's force) is also generated, which makes the device more effective. They succeeded in sorting neuroblastoma and glioma cells with 80% efficiency and high relative viability.

The effects of cancer cell-RBC interactions on the inertial migration forces were investigated by Tanaka *et al.*[141] using a non-dilute suspension of RBCs. The volume fraction of RBCs, i.e., hematocrit (Hct), used in the study varied from 0% to a concentrated regime (40%) where the cell-cell interactions significantly affected the cells' migration behavior. The strength of the inertial effect can also be estimated by the particle Reynolds number, defined as $Re_p = \rho w^2\dot{\gamma}/\mu$, where ρ is the density, w is the channel width, $\dot{\gamma}$ is the shear rate, and μ is the viscosity. When Re_p is larger than unity, the inertia effect becomes dominant.

Tanaka *et al.*[141] first investigated the migration of cancer cells in phosphate-buffered saline, i.e., Hct = 0%, to simply observe the migration phenomena. They further investigated the effect of hematocrit levels on the migration of cancer cells in a suspension of RBCs. The results indicated that the effect of RBCs on the migration of cancer cells was almost negligible when Hct = 0.1 and 1%. However, when Hct = 10 and 40%, the migrations were significantly disturbed by the interactions with RBCs. These findings are important for design optimization of microfluidic devices for future CTC testing.

Bhagat *et al.*[15] developed a microfluidic device for separating cancer cells from blood. They used the inertial migration in high aspect-ratio microchannels coupled with pinched flow dynamics. They succeeded in isolating cancer cells from a blood sample, and achieved 10^5 fold enrichment over RBCs and 10^4 fold enrichment over peripheral blood leukocytes.

Tanaka *et al.*[142] also developed a sophisticated microchannel for separating cancer cells from a suspension of RBCs, as shown in Fig. 5. The device again

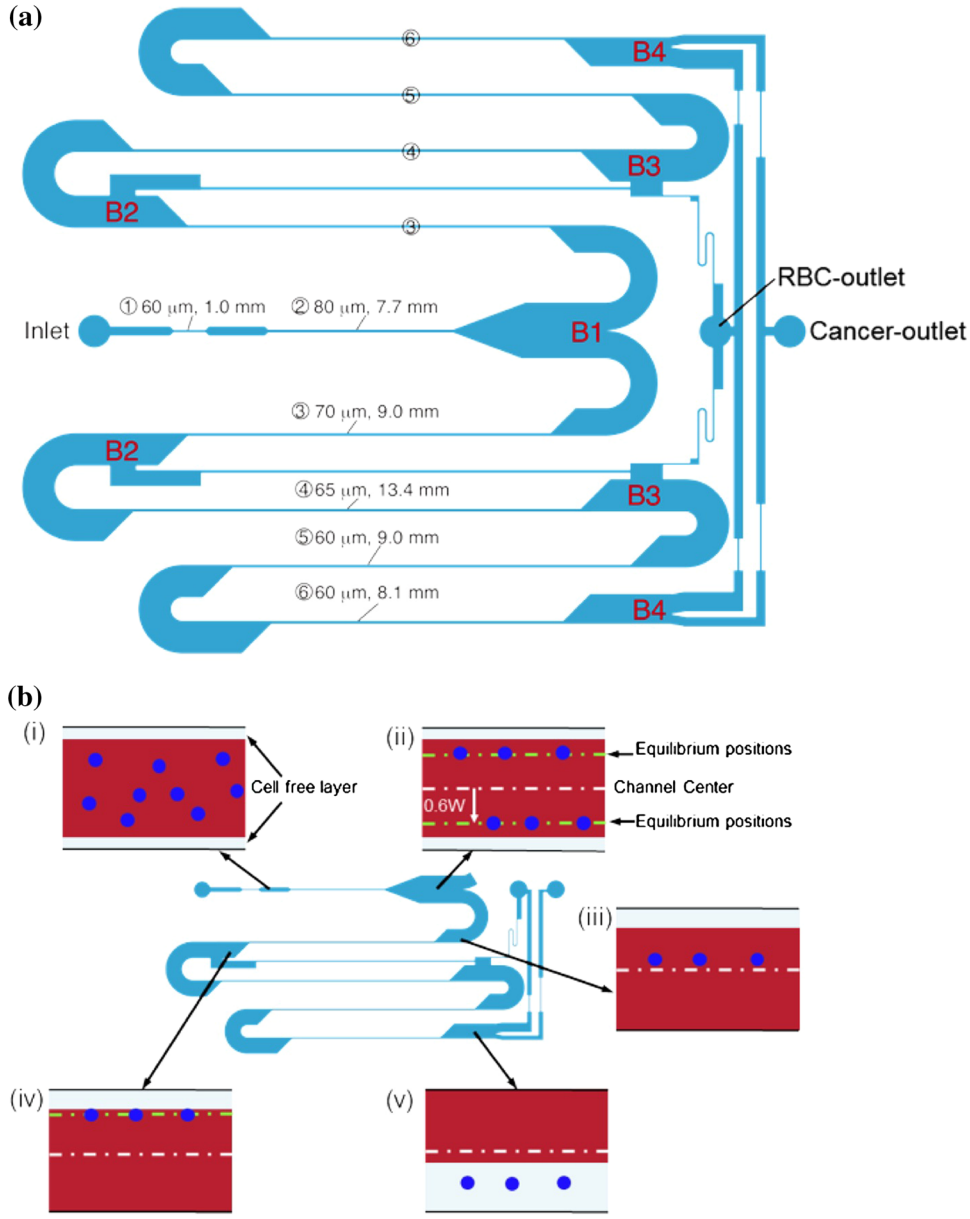

FIGURE 5. Schematic of the multistage microchannel system to separate cancer cells from a suspension of red blood cells:[142] (a) geometry (width and length) of the device and (b) separation principle of cancer cells from an RBC suspension. Cancer cells migrated towards their equilibrium positions after flowing through narrow channels due to the inertial forces. In the third narrow channel (iv), cancer cells migrated towards only one side of the channel, because the equilibrium position existed 0.6W away from the center, where W is the half width. At the second bifurcation (B2), an RBC suspension without cancer cells was extracted towards RBC-outlet. Such successive operations resulted in a reduction in the overlap between cancer cells and RBCs. Finally, only cancer cells flowed into cancer-outlet.

used the inertial migration forces, and was able to effectively separate cancer cells up to 1% hematocrit condition. The collection efficiency of cancer cells was about 85%, and the enrichment ratio was about 120-fold. These studies illustrate that the separation of cancer cells from a blood sample is possible using label-free inertial forces, thus paving the way for the development of microfluidic devices for future CTC tests.

Microfluidic Devices for Cell Adhesion

Adhesion phenomena on blood vessel walls have been intensively investigated for leukocytes, cancer cells, and malaria-infected RBCs, as mentioned in "Computational Modeling of Cellular Adhesion" section. Most of the classical *in vitro* experiments used simple channel geometries, such as straight circular or rectangular tubes, and investigated the effects of wall

shear stress, cell-cell interactions, and adhesion molecules. Recently, more realistic channel geometries have been used by some groups to identify probable adhesion sites in the microcirculation.

Ishikawa *et al.*[68] investigated the adhesion of cancer cells around symmetric bifurcations and confluences. They found that cancer cells frequently adhered to the inner wall of the bifurcation but rarely to other locations. The asymmetric tendency could not be explained by wall shear stress, because the wall shear stress was almost symmetric for the bifurcation and the confluence. They found that the distance between the cancer cell and the wall played an important role in the cell adhesion, which was strongly dependent on the channel geometry. Wang *et al.*[152] developed a microdevice with complex geometry, in which endothelium cells were cultured. They investigated the adhesive interactions between breast cancer cells and endothelial cells. The results showed signal-promoted and region-preferred adhesion of cancer cells. Antia *et al.*[7] investigated rolling motion of IRBCs at confluences, because adhesion of IRBCs has been reported frequently around confluences. They found increased accumulation of IRBCs in the branches of a model capillary network relative to the main artery. These results illustrate that microfluidic devices can be useful tools for investigating cell adhesion phenomena.

SUMMARY

In this paper, we reviewed recent computational and experimental studies of hemodynamics in microcirculation and microfluidics. As shown in "Cellular-Scale Computational Hemodynamics" section, detailed mechanical modeling of RBCs has been reported in recent papers. Using developed computational RBC models, the single cellular-level mechanics of an RBC, such as its kinematic motion under fluid flow, are now widely discussed. Recently, cellular flow in a large capillary has been simulated, and is has been found that the cell-free layer strongly affects the local shear rate and local RBC deformation, especially when the vessel diameter is over 100 μm. In addition to RBC dynamics, cell adhesion behavior has been computed by several groups. Three-dimensional stochastic adhesion models have been developed, and the computational parameters of ligand-receptor bindings, such as the dissociation rate, have been obtained from recent experimental data. Although some computational models have been compared to experimental results, there are still few experimental data on the adhesive dynamics at the cellular scale for any such comparisons. We also reviewed recent experimental PIV/PTV techniques for observation of individual RBC behavior in microfluidics. In recent years, spatial and time resolution has gradually improved, allowing for more detailed observation of cell behavior under fluid flow. This fundamental knowledge of hemodynamics can be used for biomedical applications, such as cell separation devices, as shown in "Application of hemodynamics to microfluidic devices" section. Although cell-level hemodynamics is a fast-evolving research field in biomechanics and bioengineering, the multi-scale problem remains a big challenge. In particular, there are still few transversal studies that connect molecular- and cellular-scale hemodynamics. We expect to develop a model that can express biological functions using mechanics by integrating nano, micro, and macroscopic hemodynamics, in the near future.

REFERENCES

[1]Abkarian M., M. Faivre, and A. Viallat. Swinging of red blood cells under shear flow. *Phys. Rev. Lett*. 98:188302, 2007.
[2]Adrian R. J. Particle-imaging techniques for experimental fluid mechanicsk. *Annu. Rev. Fluid Mech.,* 23:261–304, 1991.
[3]Alizadehrad D., Y. Imai, K. Nakaaki, T. Ishikawa, and T. Yamaguchi, Parallel simulation of cellular flow in microvessels using a particle method. *J. Biomech. Sci. Eng*. 7:57–71, 2012.
[4]Alizadehrad D., Y. Imai, K. Nakaaki, T. Ishikawa, and T. Yamaguchi. Quantification of red blood cell deformation at high-hematocrit blood flow in microvessels. *J. Biomech*. 45:2684–2689, 2012.
[5]AlMomani, T., H. S. Udaykumar, J. S. Marshall, and K. B. Chandran. Micro-scale dynamic simulation of erythrocyte-platelet interaction in blood flow. *Ann. Biomed. Eng*. 36: 905–920, 2008.
[6]Alon R., S. Chen, R. Fuhlbrigge, K. D. Puri, and T. A. Springer. The kinetics and shear threshold of transient and rolling interactions of L-selectin with its ligand on leukocytes. *Proc. Natl. Acad. Sci. USA* 95: 11631–11636, 1998.
[7]Antia M., T. Herricks, and P. K. Rathod. Microfluidic modeling of cell-cell interactions in malaria pathogenesis. *PLoS Pathogens* 3: e99, 2007.
[8]Artoli A. M. A. Sequeira, A. S. Silva-Herdade, and Saldanha C. Leukocytes rolling and recruitment by endothelial cells: Hemorheological experiments and numerical simulations. *J. Biomech*. 40: 3493–502, 2007.
[9]Arya M., A. B. Kolomeisly, G. M. Romo, M. A. Cruz, J.A. López, and B. Anvari. Dynamic force spectroscopy of glycoprotein Ib-IX and von Willebrand factor. *Biophys. J*. 88: 4391–4401, 2005.
[10]Asmolov, E. S., The inertial lift on a spherical particle in a plane Poiseuille flow at large channel Reynolds number. *J. Fluid Mech*., 381, 63–87, 1999.
[11]Bagchi P., Mesoscale simulation of blood flow in small vessels. *Biophys. J*., 92:1858–1877, 2007.
[12]Barthès-Biesel D., A. Diaz, and E. Dhenin. Effect of constitutive laws for two-dimensional membranes on

flow-induced capsule deformation. *J. Fluid Mech.* 460:211–222, 2002.
[13]Bell G.I. Models for the specific adhesion of cells to cells. *Science* 200: 618–627, 1978.
[14]Bhagat, A. A. S., S. S. Kuntaegowdanahalli, and I. Papautsky. Inertial microfluidics for continuous particle filtration and extraction. *Microfluid Nanofluid*, 7:217–226, 2009.
[15]Bhagat, A. A. S., H. W. Hou, and L. D. Li et al. Pinched flow coupled shear-modulated inertial microfluidics for high-throughput rare blood cell separation. *Lab Chip*, 11:1870–1878, 2011.
[16]Budd, G. T., M. Cristofanilli, and M. J. Ellis et al. Circulating tumor cells versus imaging-predicting overall survival in metastatic breast cancer. *Clin. Cancer Res.* 12:6403–6409, 2006.
[17]Carlo, D. D., J. F. Edd, and D. Irimia, et al. Equilibrium separation and filtration of particles using differential inertial focusing. *Anal. Chem.* 80:2204–2211, 2008.
[18]Carlo. D. D., Inertial microfluidics. *Lab Chip*, 9:3038–3046, 2009.
[19]Chang K. -C., D. F. J. Tees, and D. A.Hammer. The state diagram for cell adhesion under flow: leukocyte rolling and firm adhesion. *Proc. Natl. Acad. Sci. USA* 97:11262–11267, 2000.
[20]Chayer B., K. L. Pitts, G. Cloutier, and M. Fenech. Velocity measurement accuracy in optical microhemodynamics: experiment and simulation. *Physiol. Meas.* 33:1565–1602, 2012.
[21]Chen, C.-Y., P. Menon, W. Kowalski, and K. Pekkan. Time-resolved OCT-PIV: a new microscopic PIV technique for noninvasive depth-resolved pulsatile flow profile acquisition. *Exp Fluids* 54:1–9, 2012.
[22]Chen, X., D. F. Cui, C. C. Liu, and H. Li. Microfluidic chip for blood cell separation and collection based on crossflow filtration. *Sens. Actuators B*, 130:216–221, 2008.
[23]Colace, T.V., G. W. Tormoen, O. J. T. McCarty, and S. L Diamond. Microfluidics and Coagulation Biology. *Annu. Rev. Biomed. Eng.* 15:283–303, 2013.
[24]Cordasco, D., P. Bagchi. Orbital drift of capsules and red blood cells in shear flow. *Phys. Fluids* 25:091902, 2013.
[25]Cristofanilli, M., D. F. Hayes, and G. T. Budd et al. Circulating tumor cells: a novel prognostic factor for newly diagnosed metastatic breast cancer. *J. Clin. Oncol.* 23, 1420–1430, 2005.
[26]Crowl, L. M., and A. L. Fogelson. Analysis of mechanics for platelet near-wall excess under arterial blood flow conditions. *J. Fluid. Mech.* 676:348–375, 2011.
[27]Dao, M., C.T. Lim, and S. Suresh. Mechanics of the human red blood cell deformed by optical tweezers. *J. Mech. Phys. Solids.* 51:2259–2280, 2003.
[28]Dembo, M., D.C. Torney, K. Saxman, and D. Hammer. The reaction-limited kinetics of membrane-to-surface adhesion and detachment. *Proc. R. Soc. Lond. B.* 234:55–83, 1988.
[29]Doddi S. K., and P. Bagchi. Three-dimensional computational modeling of multiple deformable cells flowing microvessels. *Phys. Rev. E.* 79:046318, 2009.
[30]Dong, C., J. Cao, E. J. Struble, and H. H. Lipowsky. Mechanics of leukocyte deformation and adhesion to endothelium in shear flow. *Ann. Biomed. Eng.* 27:298–312, 1999.
[31]Dupin, M. M., I. Halliday, C. M. Care, L. Alboul and L. L. Munn. Modeling the flow of dense suspensions of deformable particles in three dimensions. *Phys. Rev. E* 75:066707, 2007.
[32]Dupire J., M. Socol, and A. Viallat. Full dynamics of a red blood cell in shear flow. *Proc. Natl. Acad. Sci. USA.* 109:20808, 2012.
[33]Dupont C., A. -V. Salsac, and D. Barthès-Biesel. Off-plane motion of a prolate capsule in shear flow. *J. Fluid Mech.* 721:180–198, 2013.
[34]Einstein A. Berichtigung zu meiner Arbeit: Eine neue Bestimmung der Moleküldimensionen. *Annalen der Physi* 591, 1905.
[35]Esposito A., J. -B. Choimet, J. N. Skepper, J. M. A. Mauritz, V. L. Lew, C. F. Kaminski, and T. Tiffert. Quantitative imaging of human red blood cells infected with *Plasmodium falciparum*. *Biophys. J.* 99:953–960, 2010.
[36]Evans E. A., and Y. C. Fung. Improved measurements of the erythrocyte geometry. *Microvasc. Res.* 4:335–347, 1972.
[37]Evans E. A., and R. Skalak. Mechanics and thermodynamics of biomembranes. Boca Raton: CRC Press, 1980.
[38]Evans E., and A. Yeung. Apparent viscosity and cortical tension of blood granulocytes determined by micropipet aspiration. *Biophys. J.* 56:151–160, 1989.
[39]Fedosov D. A., B. Caswell, S. Suresh, and G. E. Karniadakis. Quantifying the biophysical characteristics of *Plasmodium-falciparum*-parasitized red blood cells in microcirculation. *Proc. Natl. Acad. Sci. USA* 108:35–39, 2011.
[40]Fedosov D. A., B. Caswell, and G. E. Karniadakis. Wall shear stress-based model for adhesive dynamics of red blood cells in malaria. *Biophys. J.* 100:2084–2093, 2011.
[41]Fedosov, D. A., and G. Gompper. White blood cell margination in microcirculation. *Soft Matter* 10:2961–2970, 2014.
[42]Fenech, M., D. Garcia, H. J. Meiselman, and G. Cloutier. A particle dynamic model of red blood cell aggregation kinetics. *Ann. Biomed. Eng.* 37:2299–2309, 2009.
[43]Fischer T. M. The red cell as a fluid droplet: tank-tread like motion of the human erythrocyte membrane in shear flow. *Science* 202:894–896, 1978.
[44]Fischer T. M. Is the surface area of the red cell membrane skeleton locally conserved?. *Biophys. J.* 61:298–305, 1992.
[45]Fogelson, A. L., and R. D. Guy. Platelet-wall interactions in continuum models of platelet thrombosis: formulation and numerical solution. *Math. Med. Biol.* 21:293–334, 2004.
[46]Freund, J. B. Leukocyte margination in a model microvessel. *Phys. Fluids* 19:023301, 2007.
[47]Freund J. B., and M. M. Orescanin. Cellular flow in a small blood vessel. *J. Fluid Mech.* 671:466–490, 2011.
[48]Freund J. B. Numerical simulation of flowing blood cells. *Ann. Rev. Fluid Mech.* 46:67–95, 2014.
[49]Fu, Y., R. Kunz, J. Wu, and C. Dong. Study of local hydrodynamic environment in cell-substrate adhesion using side-view μPIV technology. *PLoS ONE.* 7:e30721, 2012.
[50]Galdi, G. P., A, Robertson, R. Rannacher, and S. Turek. Hemodynamical flows: modeling, analysis and simulations. *Birkhauser*, 2002.
[51]Glenister F. K., R. L. Coppel, A. F. Cowman, N. Mohandas, and B. M. Cooke. Contribution of parasite proteins to altered mechanical properties of malaria-infected red blood cells. *Blood* 99: 1060–1063, 2002.

[52]Green A. E., and J. E. Adkins. Large Elastic Deformation. Oxford: Clarendon Press.
[53]Goldsmith H. L., and S. Spain. Margination of leukocytes in blood flow through small tubes. *Microvasc. Res.* 27: 204–222, 1984.
[54]Gorkin, R., J. Park, J. Siegrist, et al. Centrifugal microfluidics for biomedical applications. *Lab Chip*, 10:1758–1773, 2010.
[55]Gossett, D. R., W. M. Weaver, and A. J. Mach et al. Label-free cell separation and sorting in microfluidic systems. *Anal. Bioanal. Chem.* 397:3249–3267, 2010.
[56]Ha, H., K. -H. Nam, and S. J. Lee . Hybrid PIV?PTV technique for measuring blood flow in rat mesenteric vessels. *Microvasc. Res.* 84:242–248, 2012.
[57]Haga, J. H., A. J. Beaudoin, J. G. White, and J. Strony . Quantification of the passive mechanical properties of the resting platelets. *Ann. Biomed. Eng.* 26: 268–277, 1998.
[58]Halliday I. et al. Multiscale interaction of particulate flow and the arterial wall. *Med. Eng. Phys.* 33:840–848, 2011.
[59]Hammer D. A. Adhesive dynamics. *J. Biomech. Eng.*136:021006, 2014.
[60]Hochmuth, R. M., H. P. Ting-Beall, B. B. Beaty, D. Needham, and R. Tran-Son-Tay. Viscosity of passive human neutrophils undergoing small deformations. *Biophys. J.* 64:1596–1601, 1993.
[61]Hogers, B., M. C. DeRuiter, A. C. Gittenberger-de Groot, and R.E. Poelmann. Extraembryonic venous obstructions lead to cardiovascular malformations and can be embryolethal. *Cardiovasc. Res.* 41:87–99, 1999.
[62]Hosseini, S. M., and J. J. Feng. How malaria parasite reduce the deformability of infected red blood cells. *Biophys. J.* 103:1–10, 2012.
[63]Hove, J. R., R. W. Köster, A. S. Forouhar, G. Acevedo-Bolton, S. E. Fraser, and M. Gharib. Intracardiac fluid forces are an essential epigenetic factor for embryonic cardiogenesis. *Nature*, 421:172–177, 2003.
[64]Hu, X. -Q., A. -V. Salsac, and D. Barthès-Biesel. Flow of a spherical capsule in a pore with circular or square cross-section. *J. Fluid Mech.* 705:176–194, 2012.
[65]Hur, S. C., H. T. K. Tse, and D. D. Carlo. Sheathless inertial cell ordering for extreme throughput flow cytometry. *Lab Chip*, 10:274–280, 2010.
[66]Imai Y., H. Kondo, T. Ishikawa, C. T. Lim, and T. Yamaguchi T. Modeling of hemodynamics arising from malaria infection. *J. Biomech.* 43:1386–1393, 2010.
[67]Imai, Y., K. Nakaaki, H. Kondo, T. Ishikawa, C. T. Lim, and T. Yamaguchi. Margination of red blood cells infected by *Plasmodium falciparum* in a microvessel. *J. Biomech.* 44: 1553–1558, 2011.
[68]Ishikawa, T. et al. Asymmetry of blood flow and cancer cell adhesion in a microchannel with symmetric bifurcation and confluence. *Biomed. Microdev.*, 13:159–167, 2011.
[69]Jadhav, S., C. D. Eggleton, and K. Konstantopoulos. A 3-d computational model predicts that cell deformation affects selectin-mediated leukocyte rolling. *Biophys. J.* 88:96–104, 2005.
[70]Kamada, H., K. Tsubota, M. Nakamura, S. Wada, T. Ishikawa, and T. Yamaguchi. A three-dimensional particle simulation of the formation and collapse of a primary thrombus. *Int. J. Numer. Method Biomed. Eng.* 26:488–500, 2010.
[71]Kamada, H., Y. Imai, M. Nakamura, T. Ishikawa, and T. Yamaguchi. Computational analysis on the mechanical interaction between a thrombus and red blood cells: Possible causes of membrane damage of red blood cells at microvessels. *Med. Eng. Phys.* 34:1411–1420, 2012.
[72]Kamada, H., Y. Imai, M. NakamuraT. Ishikawa and T. Yamaguchi. Computational study on thrombus formation regulated by platelet glycoprotein and blood flow shear. *Microvasc. Res.* 89, 95–106, 2013.
[73]Khismatullin, D. B., and G. A. Truskey. Leukocyte rolling on P-selectin: a three-dimensional numerical study of the effect of cytoplasmic viscosity. *Biophys. J.* 102:1757–1766, 2012.
[74]Kikuchi, K., and O. Mochizuki. Micro-PIV measurements in micro-tubes and proboscis of mosquito. *J. Fluid Sci. Technol.* 3:975–86, 2008.
[75]Kikuchi, K., and O. Mochizuki. Micro-PIV (micro particle image velocimetry) visualization of red blood cells (RBCs) sucked by a female mosquito. *Meas. Sci. Technol.* 22:064002, 2011.
[76]Kim, S., L. R. Long, A. S. Popel, M. Intaglietta and P. C. Johnson. Temporal and spatial variations of cell-free layer width in arterioles. *Am. J. Phys.* 293:H1526–H1535, 2007.
[77]Kondo, H., Y. Imai, T. Ishikawa, K. Tsubota, and T. Yamaguchi. Hemodynamic analysis of microcirculation in malaria infection. *Ann. Biomed. Eng.* 37:702–709, 2009.
[78]Koutsiaris, A. G, and A. Pogiatzi. Velocity pulse measurements in the mesenteric arterioles of rabbits. *Physiol. Meas.* 25:15–25, 2004.
[79]Kuntaegowdanahalli, S. S., A. A. S. Bhagat et al. Inertial microfluidics for continuous particle separation in spiral microchannels. *Lab Chip* 9:2973–2980, 2009.
[80]Lac, E., D. Barthès-Biesel, N. A. Pelekasis, and J. Tsamopoulos. Spherical capsules in three-dimensional unbounded Stokes flows: effect of the membrane constitutive law and onset of buckling. *J. Fluid Mech.* 516:303–334, 2004.
[81]Le, D.-V., and Z. Tan. Large deformation of liquid capsules enclosed by thin shells immersed in the fluid. *J. Comput. Phys.* 229:4097–4116, 2010.
[82]Lee, J. Y., H. S. Ji, and S. J. Lee. Micro-PIV measurements of blood flow in extraembryonic blood vessels of chicken embryos. *Physiol. Meas.* 28:1149, 2007.
[83]Lefebvre, Y., E. Leclerc, D. Barthes-Biesel, J. Walter and F. Edwards-Levy. Flow of artificial capsules in microfluidic channels: a method for determining the elastic properties of the membrane. *Phys. Fluids* 20:123102, 2008.
[84]Lei, H., D. A. Fedosov, B. Caswell, and G. M. Karniadakis. Blood flow in small tubes: quantifying the transition to the non-continuum regime. *J. Fluid Mech.* 722:214–239, 2013.
[85]Li, A., A. H. Mansoor, K. S. W. Tan, and C. T. Lim. Observations on the internal and surface morphology of malaria infected blood cells using optical and atomic force microscopy. *J. Microbiol. Method.* 66: 434–439, 2006.
[86]Li, A., T. S. Lim, H. Shi, S. J. Tan, Z. Li, B. C. Low, K. S. W. Tan, and C. T. Lim. Molecular mechanic insights into the endothelial receptor mediated cytoadherence of *Plasmodium falciparum*-infected erythrocytes. *PLoS ONE* 6:e16929, 2011.
[87]Li, J., G. Lykotrafitis, M. Dao, and S. Suresh. Cytoskeletal dynamics of human erythrocyte. *Proc. Natl. Acad. Sci. USA*. 104:4937–4942, 2007.
[88]Lima, R, C. S. Fernandes, R. Dias, T. Ishikawa, Y. Imai, and T. Yamaguchi. Microscale Flow Dynamics of Red Blood Cells in Microchannels: An Experimental and Numerical Analysis. Berlin: Springer, pp. 297–309, 2011.

[89]Mach, A. J., and D. D. Carlo. Continuous scalable blood filtration device using inertial microfluidics. *Biotechnol. Bioeng*. 107:302–311, 2010.
[90]Magowan, C., W. Wollish, L. Anderson, and J. Leech. Cytoadherence by *Plasmodium falciparum*-infected erythrocytes is correlated with the expression of a family of variable proteins on infected erythrocytes. *J. Exp. Med.* 168:1307–1320, 1988.
[91]McWhirter, J. L., H. Noguchi, and G. Gompper. Flow-induced clustering and alignment of vesicles and red blood cells in microcapillaries. *Proc. Natl. Acad. Sci. USA*. 106:6039–6043, 2009.
[92]Meinhart, C. D., S. T. Wereley, and J. G. Santiago. PIV measurements of a microchannel flow. *Exp. Fluids* 27:414–419, 1999.
[93]Meinhart, C. D, S. T. Wereley, and M. H. B. Gray. Volume illumination for two-dimensional particle image velocimetry. *Meas. Sci. Technol.* 11:809–814, 2000.
[94]Miller, L. H., D. I. Baruch, K. Marsh, and O. K. Doumbo. The pathogenic basis of malaria. *Nature* 415:673–679, 2002.
[95]Miyazaki, H., and T. Yamaguchi. Formation and destruction of primary thrombi under the influence of blood flow and von Willebrand factor analyzed by a discrete element method. *Biorheology* 40:265–272, 2002.
[96]Mody, N. A., and M. R. King. Platelet adhesive dynamics. Part II: high shear-induced transient aggregation via GPIb-vWF-GPIb bindings. *Biophys. J.* 95:2556–2574, 2008.
[97]Mohandas, N., and P. G. Gallagher. Red cell membrane: past, present, and future. *Blood* 112:3939–3948, 2008.
[98]Moon, H. -S., K. Kwon, S. -I. Kim et al. Continuous separation of breast cancer cells from blood samples using multi-orifice flow fractionation (MOFF) and dielectrophoresis (DEP). *Lab Chip* 11:1118–1125, 2011.
[99]Mori, D., K. Yano, K. Tsubota, T. Ishikawa, S. Wada, and T. Yamaguchi. Simulation of platelet adhesion and aggregation regulated by fibrinogen and von Willebrand factor. Thromb. Haemost. 99:108–115, 2008.
[100]Mori, D., K. Yano, K. Tsubota, T. Ishikawa, S. Wada, and T. Yamaguchi. Computational study on the effect of red blood cells on primary thrombus formation. *Thromb. Res.* 123:114–121, 2008.
[101]Navot, Y. Elastic membranes in viscous shear flow. *Phys. Fluids* 10:1819–1833, 1998.
[102]N'Dri, N. A., W. Shyy, and R. Tran-Son-Tay. Computational modeling of cell adhesion and movement using a continuum-kinetics approach. *Biophys. J.* 85:2273–2286, 2003.
[103]Needham, D., and R. M. Hochmuth. A sensitive measure of surface stress in the resting neutrophil. Biophys. J. 61:1664–1670, 1992.
[104]Noguchi, H. Swinging and synchronized rotations of red blood cells in simple shear flow. Phys. Rev. E 80:021902, 2009.
[105]Nobis, U., A. R. Pries, G. R. Cokelet, and P. Gaehtgens. Radial distribution of white cells during blood flow in small tubes. *Mirovasc. Res.* 29:295–304, 1985.
[106]Olsen, M. G., and R. J. Adrian. Out-of-focus effects on particle image visibility and correlation in microscopic particle image velocimetry. *Exp. Fluids.* 29:S166–S74, 2000.
[107]Omori, T., T. Ishikawa, D. Barthès-Biesel, A. -V. Salsac, J. Walter, Y. Imai, and T. Yamaguchi. Comparison between spring network models and continuum constitutive laws: application to the large deformation of a capsule in shear flow. *Phys. Rev. E.* 83:041918, 2011.
[108]Omori, T., T. Ishikawa, Y. Imai, T. Yamaguchi, and T. Ishikawa. Reorientation of a nonspherical capsule in creeping shear flow. *Phys. Rev. Lett.* 108:138102, 2012.
[109]Omori, T., T. Ishikawa, D. Barthès-Biesel, A. -V. Salsac, Y. Imai, and T. Yamaguchi. Tension of red blood cell membrane in simple shear flow. *Phys. Rev. E* 86:056321, 2012.
[110]Pappu, V., and P. Bagchi. 3D computational modeling and simulation of leukocyte rolling adhesion and deformation, *Comput. Biol. Med.* 38:738–753, 2008.
[111]Park, J. S., C. K. Choi, and K. D. Kihm. Optically sliced micro-PIV using confocal laser scanning microscopy (CLSM). *Exp. Fluids* 37:105–19, 2004.
[112]Park, J. S., S. H. Song, and H. I. Jung. Continuous focusing of microparticles using inertial lift force and vorticity via multi-orifice microfluidic channels. *Lab Chip* 9:939–948, 2009.
[113]Peng, Z., A. Mashayekh, and Q. Zhu. Erythrocyte responses in low-shear-rate flows: effect of non-biconcave stress-free state in the cytoskeleton. *J. Fluid Mech.* 742:96–118, 2014.
[114]Petersson, F., A. Nilsson, C. Holm et al. Separation of lipids from blood utilizing ultrasonic standing waves in microfluidic channels. *Analyst* 129:938–943, 2004.
[115]Pickard, J. E., and K. Ley. Micro-PTV Measurement of the fluid shear stress acting on adherent leukocytes in vivo. *Biophys. J.* 96:4249–59, 2009.
[116]Pitts, K. L., R. Mehri, C. Mavriplis, and M. Fenech. Micro-particle image velocimetry measurements of blood flow: Validation and analysis of data post-processing methods. *Meas. Sci. Technol.* 23:105302, 2012.
[117]Pitts, K. L., and M. Fenech. High speed versus pulsed images for micro-particle image velocimetry: a direct comparison of red blood cells versus fluorescing tracers as tracking particles. *Physiol. Meas.* 34:1363–1374, 2013.
[118]Pivkin, I. V., P. D. Richardson, and G. Karniadakis. Blood flow velocity effects and role of activation delay time on growth and form of platelet thrombi. *Proc. Natl. Acad. Sci. USA* 103:17164–17169, 2006.
[119]Pivkin, I., P. Richardson and G. Karniadakis. Effect of red blood cells on platelet aggregation. *IEEE Eng. Med. Biol. Mag.* 28:32–37, 2009.
[120]Poelma, C., P. Vennemann, R. Lindken, and J. Westerweel. In vivo blood flow and wall shear stress measurements in the vitelline network. *Exp. Fluids*, 45:703–13, 2008.
[121]Poelma, C., A. Kloosterman, B. P. Hierck, and J. Westerweel. Accurate blood flow measurement: Are artificial tracers necessary? *PLOS ONE*, 7:e45247, 2012.
[122]Pontrelli, G., I. Halliday, S. Melchionna, T. J. Spencer, and S. Succi. Lattice Boltzmann method as a computational framework for multiscale haemodynamics. *Math. Comp. Model Dyn. Syst.*, 20:470–490, 2014.
[123]Pontrelli, G., I. Halliday, S. Melchionna, T. J., Spencer C. S. Konig, and M. W. Collins. Modelling the glycocalyx-endothelium-erythrocyte interaction in the microcirculation: a computational study. *Comput. Meth. Biomech. Biomed. Eng*. in press, 2013.
[124]Popel, A. S., and P. C. Johnson. Microcirculation and Hemorheology. *Annu. Rev. Fluid Mech.* 2005: 37:43–68, 2005.
[125]Pozrikidis, C. Modeling and Simulation of Capsules and Biological Cells. Boca Raton: Chapman & Hall/CRC, 2003.

[126]Pratt, E. D., Huang, C., Hawkins, B. G., et al. Rare cell capture in microfluidic devices. *Chem. Eng. Sci.* 66:1508–1522, 2011.
[127]Pries, A. R., D. Neuhaus, and P. Gaehtgens. Blood viscosity in tube flow: dependence on diameter and hematocrit. *Am. J. Phys.* 263:H1770–H1778, 1992.
[128]Pries, A. R., and T. W. Secomb. Modeling structural adaptation of microcirculation. *Microcirculation* 15:753–764, 2008.
[129]Ramanujan, S., and C. Pozrikidis. Deformation of liquid capsules enclosed by elastic membranes in simple shear flow: large deformations and the effect of fluid viscosities. *J. Fluid Mech.* 361:117–143, 1998.
[130]Ruggeri, Z. M., and G. L. Mendolicchio. Adhesion mechanisms in platelet function. *Circ. Res.* 100:1673–85, 2007.
[131]Santiago, J., S. Wereley, C. Meinhart, D. Beebe, and R. Adrian. A particle image velocimetry system for microfluidics. *Exp. Fluids* 25:316–9, 1998.
[132]Schmid-Schönbein, G. W., S. Usami, R. Skalak and S. Chien. The interaction of leukocytes and erythrocytes in capillary and postcapillary vessels. *Microvasc. Res.* 19:45–70, 1980.
[133]Skalak, R., A. Tozeren, P. R. Zarda, and S. Chien. Strain energy function of red blood cell membranes. *Biophys. J.* 13:245–264, 1973.
[134]Skotheim, J. M., and T. W. Secomb. Red blood cells and other nonspherical capsules in shear flow: oscillatory dynamics and the tank-treading-to-tumbling transition. *Phys. Rev. Lett.* 98:078301, 2007.
[135]Smith, M. J., E. L. Berg, and M. B. Lawrence. A direct comparison of selectin-mediated transient, adhesive events using high temporal resolution. *Biophys. J.* 77:3371–3383, 1999.
[136]Sugii, Y., S. Nishio and K. Okamoto. In vivo PIV measurement of red blood cell velocity field in microvessels considering mesentery motion. *Physiol. Meas.* 23:403–426, 2002.
[137]Sugii, Y., R. Okuda, K. Okamoto, H. Madarame. Velocity measurement of both red blood cells and plasma of in vitro blood flow using high-speed micro PIV technique. *Meas. Sci. Technol.*, 16:1126, 2005.
[138]Sui, Y., Y. T. Chew, P. Roy, Y. P. Cheng and H. T. Low. Dynamic motion of red blood cells in simple shear flow. *Phys. Fluids* 20:112106, 2008.
[139]Suresh, S., J. Spatz, J. P. Mills, A. Micoulet, M. Dao, C. T. Lim, M. Beil, and T. Seufferlein. Connections between single-cell biomechanics and human disease states: gastrointestinal cancer and malaria. *Acta Biomater.* 1:15–30, 2005.
[140]Takeishi, N., Y. Imai, K. Nakaaki, T. Yamaguchi and T. Ishikawa. Leukocyte margination at arteriole shear rate. *Physiol. Rep.* 2:e12037, 2014.
[141]Tanaka, T., T. Ishikawa, K. Numayama-Tsuruta, et al. Inertial migration of cancer cells in blood flow in microchannels. *Biomed. Microdev.* 14:25–33, 2012.
[142]Tanaka, T., T. Ishikawa, K. Numayama-Tsuruta et al. Separation of cancer cells from a red blood cell suspension using inertial force. *Lab Chip* 12:4336–4343, 2012.
[143]Tangelder G. J., D. W. Slaaf, T. Arts, and R. S. Reneman. Wall shear rate in arterioles in vivo: least estimates from platelet velocity profiles. *Am. J. Physiol.*, 254:H1059–H64, 1988.
[144]Tangelder, G. J., H. C. Teirlinck, D. W. Slaaf and R. S. Reneman. Distribution of blood platelets flowing arterioles. *Am. J. Physiol. Heart Circ. Physiol.* 248:H318–H323, 1985.
[145]Ting-Beall, H. P., D. Needham, and R. M. Hochmuth. Volume and osmotic properties of human neutrophils. *Blood* 81:2774–2780, 1993.
[146]Tran-Son-Tay, R., H. -C. Kan, H. S. Udaykumar, E. Damay, and W. Shyy. Rheological modelling of leukocytes. *Med. Biol. Eng. Comput.* 36:246–250, 1998.
[147]Tsubota, K., and S. Wada. Effect of the natural state on an elastic cellular membrane on tank-treading and tumbling motions of a red blood cell. *Phys. Rev. E* 81:019910, 2010.
[148]Vennemann, P. K. T. Kiger, R. Lindken, B. C. W. Groenendijk, S. Stekelenburg-de Vos, T. L. M. ten Hagen et al. In vivo micro particle image velocimetry measurements of blood-plasma in the embryonic avian heart. *J. Biomech.* 39:1191–200, 2006.
[149]Vennemann, P., R. Lindken, J. Westerweel. In vivo whole-field blood velocity measurement techniques. *Exp. Fluids* 42:495–511, 2007.
[150]Walter, J., A.-V. Salsac, D. Barthès-Biesel, P. Le Tallec. Coupling of finite element and boundary integral methods for a capsule in a Stokes flow. *Int. J. Numer. Method Eng.* 83:829–850, 2010.
[151]Wan, J., W. D. Ristenpart, and H. A. Stone. Dynamics of shear-induced ATP release from red blood cells. *Proc. Natl. Acad. Sci. USA* 105:16432–16437, 2008.
[152]Wang, J. -C., et al. Pneumatic mold-aided construction of a three-dimensional hydrogel microvascular network in an integrated microfluidics and assay of cancer cell adhesion onto the endothelium. *Microfluid. Nanofluid.*, 15:519–532, 2013.
[153]Wang, W., and M. R. King. Multiscale modeling of platelet adhesion and thrombus growth. *Ann. Biomed. Eng.* 40:2345–2354, 2012.
[154]Wang, W., T. G. Diacovo, J. Chen, J. B. Freund, and M. R. King. Simulation of platelet, thrombus and erythrocyte hydrodynamic interactions in a 3D arteriole with in vivo comparison. *PLoS ONE* 8:e76949, 2013.
[155]Watts, T., M. Barigou, G. B. Nash. Comparative rheology of the adhesion of platelets and leukocytes from flowing blood: why are platelets so small?. *Am. J. Physiol. Heart Circ. Physiol.* 304:H1483–H1494, 2013.
[156]Wereley, S. T., J. G. Santiago, R. Chiu, C. D. Meinhart, and R. J. Adrian. Microresolution particle image velocimetry. *Proc. SPIE* 122–133, 1998.
[157]Wilhelm, S., B. Grobler, M. Gluch, and H. Heinz. Confocal Laser Scanning Microscopy. Principles. Microscopy from Carl Zeiss, Microspecial, 2003.
[158]Woldhuis, B., G. J. Tangelder, D. W. Slaaf, and S. Reneman. Concentration profile of blood platelets differs in arterioles and venules. *Am. J. Physiol. Heart Circ. Physiol.* 262:H1217–H1223, 1992.
[159]Wong, K. H. K., J. M. Chan, R. D. Kamm, and J. Tien. Microfluidic model of vascular functions. *Ann. Rev. Biomed. Eng.* 14:205–230, 2012.
[160]Wu, Z., B. Willing, J. Bjerketorp, et al. Soft inertial microfluidics for high throughput separation of bacteria from human blood cells. *Lab Chip* 9:1193–1199, 2009.
[161]Xu, Z., J. Lioi, J. Mu, M. M. Kamocka, X. Liu, D. Z. Chen, E. D. Rosen, and M. Alber. A multi-scale model of venous thrombus formation with surface-mediated control of blood coagulation cascade. *Biophys. J.* 98:1723–1732, 2010.
[162]Yang, S., A. Ündar, and J. D. Zahn. A microfluidic device for continuous, real time blood plasma separation. *Lab Chip* 6:871–880, 2006.

[163]Yoshimura, K., J. Usukura, and M. Sokabe. Gating-associated conformational changes in the mechanosensitive channel MscL. *Proc. Natl. Acad. Sci. USA* 105:4033, 2008.
[164]Zhang, J., P. C. Johnson, and A. S. Popel. Red blood cell aggregation and dissociation in shear flows simulated by lattice Boltzmann method. *J. Biomech.* 41:47–55, 2008.
[165]Zhao, H., E. S. G. Shaqfeh, and V. Narsimhan. Shear-induced particle migration and margination in a cellular suspension. *Phys. Fluids* 24:011902, 2012.
[166]Zhelev, D. V., D. Needham, and R. M. Hochmuth. Role of the membrane cortex in neutrophil deformation in small pipets. *Biophys. J.* 67:696–705, 1994.